Comput Mech (2011) 47:65–75
DOI 10.1007/s00466-010-0529-6

ORIGINAL PAPER

Study of liquid sloshing: numerical and experimental approach

Ashkan Rafiee · Fabrizio Pistani · Krish Thiagarajan

Received: 27 January 2010 / Accepted: 8 August 2010 / Published online: 27 August 2010

Abstract In this paper, sloshing phenomenon in a rectangular tank under a sway excitation is studied numerically and experimentally. Although considerable advances have occurred in the development of numerical and experimental techniques for studying liquid sloshing, discrepancies exist between these techniques, particularly in predicting time history of impact pressure. The aim of this paper is to study the sloshing phenomenon experimentally and numerically using the Smoothed Particle Hydrodynamics method. The algorithm is enhanced for accurately calculating impact load in sloshing flow. Experiments were conducted on a 1 : 30 scaled two-dimensional tank, undergoing translational motion along its longitudinal axis. Two different sloshing flows corresponding to the ratio of exciting frequency to natural frequency were studied. The numerical and experimental results are compared for both global and local parameters and show very good agreement.

Keywords Sloshing · Lagrangian methods · Smoothed Particle Hydrodynamics (SPH) · Impact pressure

A. Rafiee (✉) · F. Pistani · K. Thiagarajan
School of Mechanical Engineering, The University of Western Australia, Crawley, WA 6009, Australia
e-mail: rafiee@mech.uwa.edu.au

F. Pistani
e-mail: fpistani@mech.uwa.edu.au

K. Thiagarajan
e-mail: Krish.Thiagarajan@uwa.edu.au

F. Pistani
INSEAN, Istituto Nazionale Studi ed Esperienze in Architettura Navale, The Italian Research Center for Ship Hydrodynamics, Milan, Italy

1 Introduction

The phenomenon of fluid motion in a partially filled tank due to the tank motion is known as sloshing. The resonant condition in sloshing, which occurs when the the frequency of tank motion is close to the natural frequency of the fluid inside it, may cause large structural loads on the tank frame. This resonance phenomenon may be connected with complex motions of the filled liquid that can couple with structure motions and can represent a danger for the tank structure and for the stability of the structure. On the other hand, at certain filling ratios it may also create high impact loads on the ceiling of the tank causing significant structural damage. Therefore identifying the behavior of the fluid flow during sloshing is crucial for the design of the tanks [1,2].

The type of excitation, the ratio of frequency to natural frequency and the amplitude, dictate the behavior of the free surface motion of the liquid inside the tank. Several forms of excitation can occur, such as impulsive, sinusoidal and random. The tank motion can be sway, roll, pitch/yaw excited or a combination of them. The resulting free surface profile can be a composition of different wave modes such as hydraulic jump and travelling waves in the mild sloshing or standing and breaking waves in severe sloshing [3–5].

In the past five decades, sloshing motion has been investigated by many researchers, using various techniques. Initial studies were based on mechanical models of the phenomenon by adjusting terms in the harmonic equation of motion [6,7] when time-efficient and reasonably accurate results were deemed sufficient [8]. Some other researchers solved the potential flow problem with very complicated treatment of free-surface boundary conditions [9]. Although the method is very accurate for specific applications, it cannot handle breaking waves and tanks with baffles. Others solved the non-linear shallow water equations [4] by means of either

Glimm's method [10] or gas analogy formulation [11], with respect to the 2D rolling problem.

The most practical method of studying sloshing physics is the experimental technique. Abramson [12] evaluated the results from model tests with tanks of various shapes and the effect of viscosity and tank shape and of various damping devices is outlined. These studies were mainly related to liquid fuel tanks on space vehicles. In the 1970s and early 1980s, the sloshing problem became an important issue in the design of the liquefied natural gas carriers. Several experimental and analytical approaches were considered during this time. A major set of experiments were performed by Bass et al. [13] during 1980s on the various parameters effecting sloshing. Results indicated that impact pressure is constant over the range of Reynolds number investigated. Thus for large amplitude sloshing, viscous forces are of secondary importance. Liquid compressibility did not have a significant effect on the measured impact pressure. Experiments conducted at reduced ambient pressure inside the tank (also known as ullage pressure) showed significant increase in impact pressures. It was concluded that ullage pressure has little effect on impact pressures until rather low pressures are reached, which were near to vapor pressure of the liquid medium.

Besides the aforementioned techniques, numerical simulations are the most important and widely adopted technique for dealing with highly non-linear problems. Frandsen [14] used the Finite Difference method for solving the non-linear potential flow in a 2D tank. Celebi and Akyildiz [15] used the finite difference method along with Volume of Fluid technique (VoF) for tracking the free-surface. Sames et al. [16], applied a commercial VoF technique to rectangular and cylindrical tanks.

An alternative class of methods for numerical simulations which has attracted much attention is the description of both the fluid and the structure motion by a Lagrangian formulation. This is partly due to the ease of implementation and also partly because of the independence of the method from the grid information. In fact, the word meshless means that in these methods there is no inherent reliance on a particular mesh topology. The promising feature of using Lagrangian techniques for both the solid and the fluid part of the problem is that it permits one to follow the motion of the fluid–solid interface and to simulate the free-surface of the fluid without any specific treatment. The Smoothed Particle Hydrodynamics (SPH) method is a meshless technique which was originally developed in 1977 by Lucy [17] and, Monaghan and Gingold [18,19]. The method uses a purely Lagrangian approach and has been successfully employed in a wide range of problems, e.g. astrophysics [20–27], fluid mechanics [28–31], solid mechanics [32–36], fluid–structure interaction [37–39] and many more.

Recently, the Smoothed Particle Hydrodynamics (SPH) method has been applied to the study of sloshing flow [40–42]. The motivation of this work is to extend the ability of the SPH method for accurately simulating the sloshing flow and calculation of the impact pressure by using a more accurate time-stepping integration and simpler treatment of the boundary conditions.

2 The SPH method

In this paper, the SPH method is used for the numerical simulation of sloshing phenomenon. Below, a brief description of the method is presented and some important implementation issues are elaborated. The reader is referred to [39] for more elaborated description.

The SPH method is based on the interpolation theory. The method allows any function to be expressed in terms of its values at a set of disordered points representing particle positions using a kernel function. The kernel function refers to a weighting function and specifies the contribution of a typical field variable, $A(r)$, at a certain position, r, in space. The kernel estimate of $A(r)$ is defined as [25,28]

$$A(\mathbf{r}) = \int_V A(\mathbf{r}')W(\mathbf{r}-\mathbf{r}', h)d\mathbf{r}' \tag{1}$$

where V represents the solution space and the smoothing length h represents the effective width of the kernel. The properties of the kernel function should satisfy the following for mass and energy conservation

$$\int_V W(\mathbf{r}-\mathbf{r}', h)d\mathbf{r}' = 1, \quad \lim_{h\to 0} W(\mathbf{r}-\mathbf{r}', h) = \delta(\mathbf{r}-\mathbf{r}'). \tag{2}$$

If $A(\mathbf{r}')$ is known only at a discrete set of N points $\mathbf{r}_1, \mathbf{r}_2, \ldots, \mathbf{r}_N$, then we approximate $A(\mathbf{r}')$ as,

$$A(\mathbf{r}') = \sum_{j=1}^{N} \delta(\mathbf{r}'-\mathbf{r}_j)A(\mathbf{r}_j)(dV)_j \tag{3}$$

where the index j denotes the particle label and particle j carries a mass m_j at position $\mathbf{r}_j$ and density ρ_j. $(dV)_j$ is the differential volume element around the point $\mathbf{r}_j$. By inserting Eq. (3) into Eq. (1), we obtain,

$$A(\mathbf{r}) = \sum_{j=1}^{N} \int \delta(\mathbf{r}-\mathbf{r}_j)A(\mathbf{r}_j)(dV)_j W(\mathbf{r}-\mathbf{r}_j, h)\, d\mathbf{r}_j \tag{4}$$

and upon integrating, we have:

$$A(\mathbf{r}) = \sum_{j=1}^{N} A(\mathbf{r}_j)W(\mathbf{r}-\mathbf{r}_j, h)(dV)_j \tag{5}$$

The final step is to express the differential volume element $(dV)_j$ as $\frac{m_j}{\rho(\mathbf{r}_j)}$. Thus, the approximation for $A(\mathbf{r})$ can be

written as:

$$A(\mathbf{r}) = \sum_{j=1}^{N} \frac{m_j}{\rho(\mathbf{r}_j)} A(\mathbf{r}_j) W(\mathbf{r} - \mathbf{r}_j, h) \tag{6}$$

The summation is over particles which lie within a circle of radius h centered at $\mathbf{r}$. The momentum equation can be written in the SPH form as

$$\left[\frac{d\mathbf{u}}{dt}\right]_i = -\sum m_j \left(\frac{P_i}{{\rho_i}^2} + \frac{P_j}{{\rho_j}^2} + \Pi_{ij}\right) \nabla_i W_{ij} \tag{7}$$

where P, m and ρ are pressure, mass and density, respectively. In the Eq. 7, Π_{ij} is the viscous force between particle i and j and calculated as [43]

$$\Pi_{ij} = -\frac{8\mu}{\rho_i \rho_j} \frac{\mathbf{u}_{ij} \cdot \mathbf{r}_{ij}}{{\mathbf{r}_{ij}}^2 + 0.01h^2} \tag{8}$$

where μ is the dynamic viscosity of the fluid. Since the quasi-incompressible form of SPH is adopted in this work, the pressure is evaluated through the most common form of equation of state for water [28,44]

$$P_i = \frac{\rho_{0i} {c_i}^2}{7} \left(\left(\frac{\rho_i}{\rho_{0i}}\right)^7 - 1\right) \tag{9}$$

To ensure incompressibility in the flow, the speed of sound should be $c_i = 10V$ where V is the maximum velocity inside the flow. This assumption ensures that the Mach number is sufficiently small to approximate a constant density fluid.

2.1 Numerical treatment of wall boundaries

In the SPH context there are several methods for modelling boundary conditions [28,45]. In this work, the boundaries are represented by fixed particles placed with the same spacing of fluid particles. The thickness of boundary in this technique should be at least equal to the compact support of the kernel used. These particles behave entirely similar to the fluid particles and contribute to the solution procedure like others. So, the pressure equation is also solved for these wall particles to calculate the increasing pressure due to the approaching fluid particles. Furthermore, this increased pressure prevents the fluid particles from penetrating the solid boundaries. Velocities of these particles are set to the velocity of the boundary at the end of each time-step.

2.2 Calculation of impact load on the wall

The free-surface shape and total forces exerted by the flow on the tank frame can be evaluated with good accuracy even with relative low resolution [42,46]. However the pressure field presents large numerical oscillations in the SPH method and therefore calculation of the impact pressure is a challenging problem. In SPH context techniques based on different approaches of dealing with boundary conditions were introduced for measuring pressure on the solid walls [40,47].

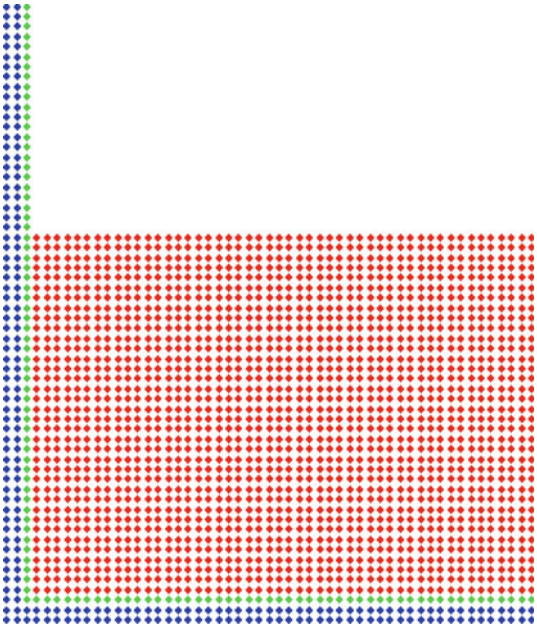

Fig. 1 The configuration of particles in 2D simulations

In this paper, a new method to measure the pressure on the solid wall, based on the boundary conditions described earlier, is presented. In this technique, one layer of fluid particles is placed on the inner layer of tank frame (Fig. 1). The fluid particles, boundary particles and particles for measuring pressure (we refer to them as pressure particles) are colored by red, blue and green, respectively. The equations of motion of the fluid are solved for these pressure particles like the fluid particles but in the SPH summation of the momentum equation 7, the sum over all neighboring particles is replaced by a sum over the only neighboring fluid particles, i.e., only the contribution of the fluid particles is considered. Therefore the force exerted to these pressure particles is only due to the momentum of fluid particles. The force is then averaged over the length that represents a typical pressure sensor diameter and eventually the pressure is calculated as:

$$P = \frac{\mathbf{F} \cdot \mathbf{n}}{D_{\text{sensor}}} \tag{10}$$

where $F \cdot n$ is the total force on the direction perpendicular to the wall and D_{sensor} is the diameter of the pressure sensor. At the end of each time-step these pressure particles are advected with the velocity of the tank frame. In three dimensional ($3D$) simulations, the same concept is used, except that D_{sensor} is replaced by the sensor cross-sectional area. Figure 2 shows the configuration of the particles in 3D simulation.

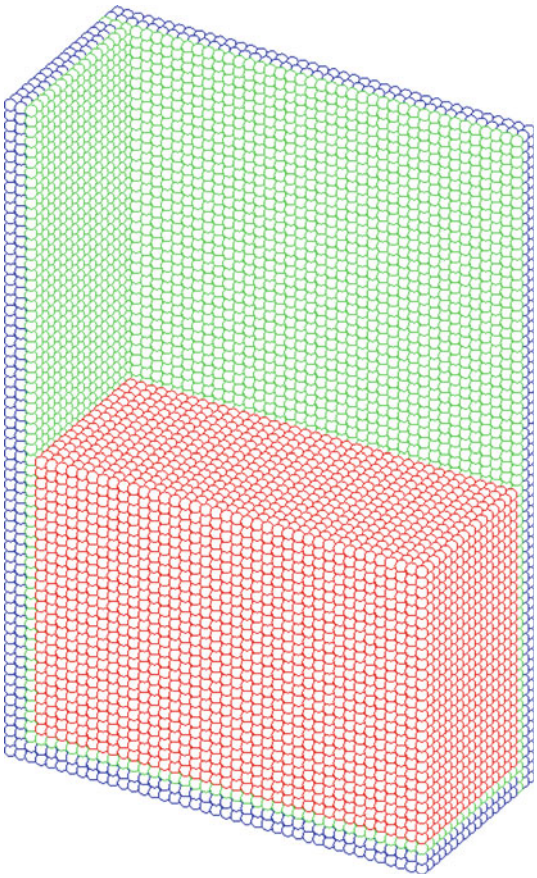

Fig. 2 The configuration of the particles in 3D simulation

3 Solution procedure

Any stable time integrating algorithm for ordinary differential equations can be used in SPH [43]. However, recently symplectic time integrators were proposed for solving the sets of ordinary equations in SPH formulation [43,48]. In this work a modified Verlet scheme which is second order accurate in time is used to integrate the set of equations describing the change of velocity $\mathbf{u}$, coordinates $\mathbf{x}$ and density ρ.

$$\begin{aligned}\left[\frac{d\mathbf{u}}{dt}\right]_i &= \mathbf{F}_i \\ \left[\frac{d\mathbf{x}}{dt}\right]_i &= \mathbf{u}_i \,. \\ \left[\frac{d\rho}{dt}\right]_i &= D_i\end{aligned} \tag{11}$$

We denote the values at the beginning of a time-step by superscript n, at the mid-point by $n+1/2$ and eventually at the end of each time-step by $n+1$. Initially, all the variable shifted to the mid-point as follows

$$\begin{cases} \mathbf{u}_i{}^{n+\frac{1}{2}} = \mathbf{u}_i{}^n + \frac{\triangle t}{2}\mathbf{F}_i{}^n \\ \mathbf{x}_i{}^{n+\frac{1}{2}} = \mathbf{x}_i{}^n + \frac{\triangle t}{2}\mathbf{u}_i{}^n \\ \rho_i{}^{n+\frac{1}{2}} = \rho_i{}^n + \frac{\triangle t}{2}D_i{}^n \end{cases} \tag{12}$$

Then the forces $\mathbf{F}_i$ are evaluated at the mid-point and the velocity and positions of particles are updated for the end of time-step by

$$\begin{cases} \mathbf{u}_i{}^{n+1} = \mathbf{u}_i{}^n + \triangle t\mathbf{F}_i{}^{n+\frac{1}{2}} \\ \qquad\qquad \Downarrow \\ \mathbf{x}_i{}^{n+1} = \mathbf{x}_i{}^{n+\frac{1}{2}} + \frac{\triangle t}{2}\mathbf{u}_i{}^{n+1} \end{cases} \tag{13}$$

Knowing the final values of velocity and position, one needs to calculate the rate of change of density and consequently the density of each particle at the end of the time-step.

$$\rho_i{}^{n+1} = \rho_i{}^{n+\frac{1}{2}} + \frac{\triangle t}{2}D_i{}^{n+1} \tag{14}$$

To speed up the calculations it is possible to use the values of $\mathbf{F}$ at previous midpoint in the predictor step. It is shown that the error introduced by this is small and of order of $O(dt^3)$ [28]. The time-step is governed by the following CFL condition

$$\triangle t \leq 0.5\frac{h}{c} \tag{15}$$

where h is the smoothing length and c represents the speed of sound in the simulation.

4 Experimental setup

The sloshing experiments are carried out in a rectangular tank partially filled with water at atmospheric pressure and room temperature. The tank dimensions are 1.3 m × 0.9 m × 0.1 m, corresponding to the length, height and width of the tank. Three of the walls are made of transparent plexiglass for optical access, while the top and one side wall are made of aluminum and host the holes for mounting the pressure sensors. On the side wall the holes are spaced 15 mm in vertical position and 25 mm in horizontal position, there are 59 vertical positions available in the central column and 31 on each of the side columns. On the top of the tank there are 3 lines of 22 holes each spaced of 15 mm and the lines are 25 mm apart (Fig. 3).

The tank is mounted on top of a motion system manufactured by MOOG. This device is capable of performing motions with six degrees of freedom.

The pressure transducers used are Kulite model XCL-8M-100-3.5BARA. They are absolute transducers, thus capable of measuring the total pressure, with a range of 3.5 bar and a diameter of the head of 2.7 mm. They use a metal diaphragm as a force collector with a piezoresistive sensor as its sensing

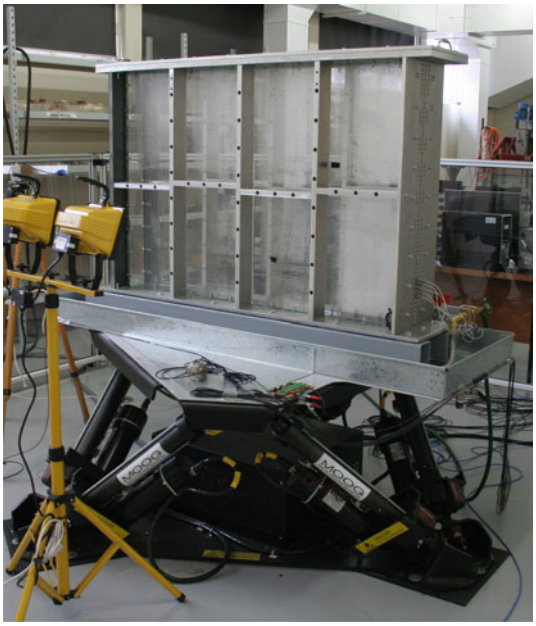

Fig. 3 The tank installed on top of the motion platform

element. The trasducers are fed with voltage of 1.25 v and the signal is amplified by a factor of 100. There is an anti-aliasing hardware filter built in the signal conditioner cards set at a cutoff frequency of 10 KHz.

The signals are acquired via Agilent U2300A data acquisition system and digitized with a resolution of 12 bit.

The position of the tank in time is measured by means of an ultrasonic position transducer, or proximity sensor, $SU1-B1$ capable of measuring distances between 0.1 and 0.6 m with a precision of ± 2mm.

A fast acquisition camera Phantom v5.2 is installed to have a view of the impact zone, the objective is a 50 mm fixed focal Nikkor lens with a maximum focal aperture of $f/1.4$. This camera has the capability of acquiring up to 1000 fps (frames per second) at the maximum resolution of 1152×896. An additional illumination of the scene has been provided in order to keep the duration of the frame as low as possible.

The setup has been designed so to synchronize the acquisition of the frames by the camera with respect of the position of tank. Sets of images of impact have been acquired during each run. These images are synchronized with the position of the tank. Based on the signal of the position sensor, a trigger is issued and a train of pulses is generated to acquire the images. The fast camera was set up so to acquire 150 images every time the trigger pulse is issued. The time interval between images was set to 0.01 s and the duration of each frame is 400 μs. The pulses that trigger the acquisition of each frame are also collected by the acquisition system making it possible to correlate each image to exact instant when it has been acquired and with the correspondent measured pressures and position of the tank. After every acquisition the memory of the camera is downloaded to the hard disk of the host computer.

5 Experimental results

The present tests have been performed for a filling level equivalent to 20% of the height of the tank, i.e. 0.18 m.

The motion base was programmed to execute a regular sinusoidal motion along the direction of the long side of the tank. The amplitude of the motion was 0.2 m peak to peak and two different frequencies have been tested, namely $f_{\text{res}} = 0.496$ Hz, that corresponds to the resonance frequency at this filling level and a lower frequency $f_{\text{low}} = 0.298$ Hz $(= 0.6 \times f_{\text{res}})$. The signals are acquired at a sampling

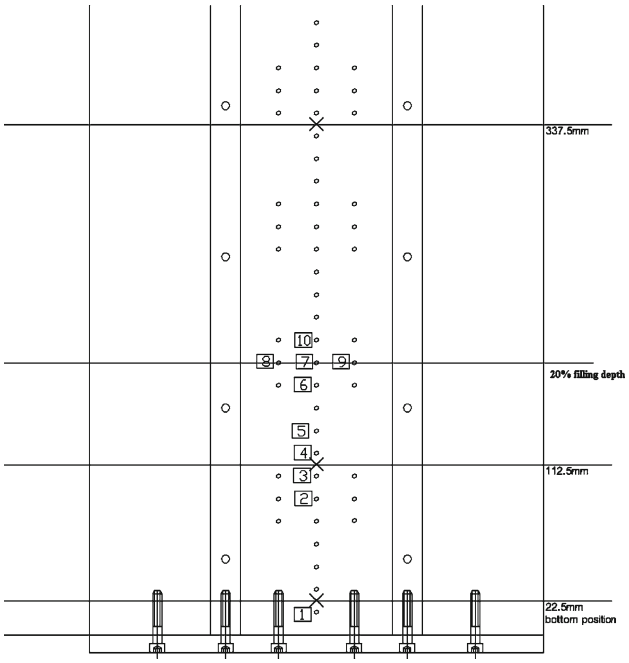

Fig. 4 Position of the pressure sensors

Table 1 Position of the pressure transducers

Sensor	Number	pos Z (mm)	pos Y (mm)
p139	1	50	15
p106	2	50	90
p100	3	50	105
p119	4	50	120
p133	5	50	135
p180	6	50	165
p084	7	50	180
p078	8	75	180
p186	9	25	180
p136	10	50	195

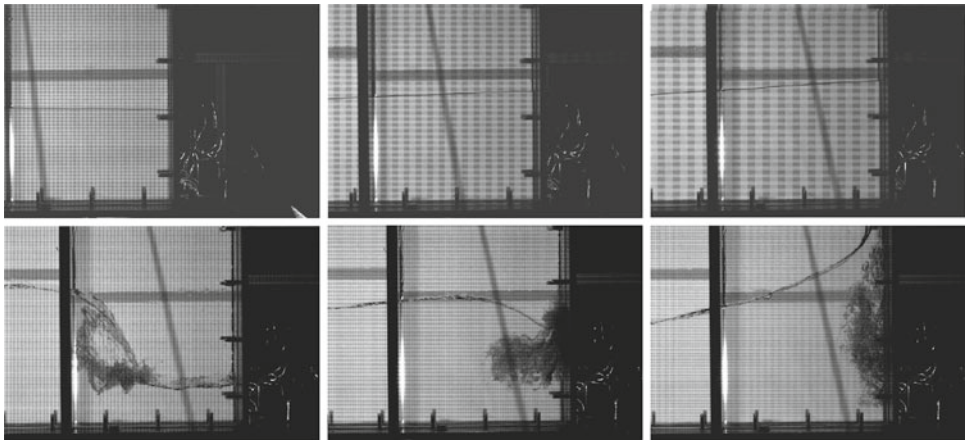

Fig. 5 The snapshots of the sloshing at the different times for $f = 0.298$ Hz (*first row*) and $f = 0.496$ Hz (*second row*)

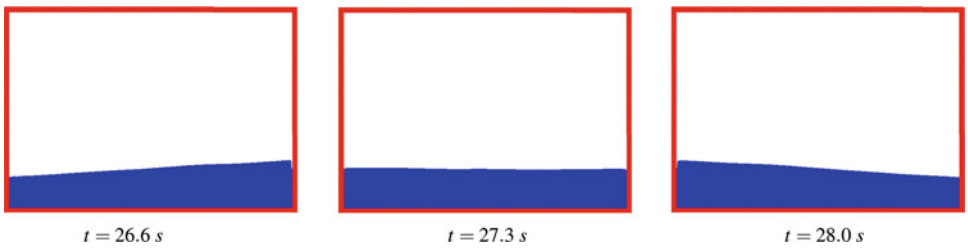

Fig. 6 The snapshots of the SPH results for sloshing flow at the different times for $f = 0.298$ Hz

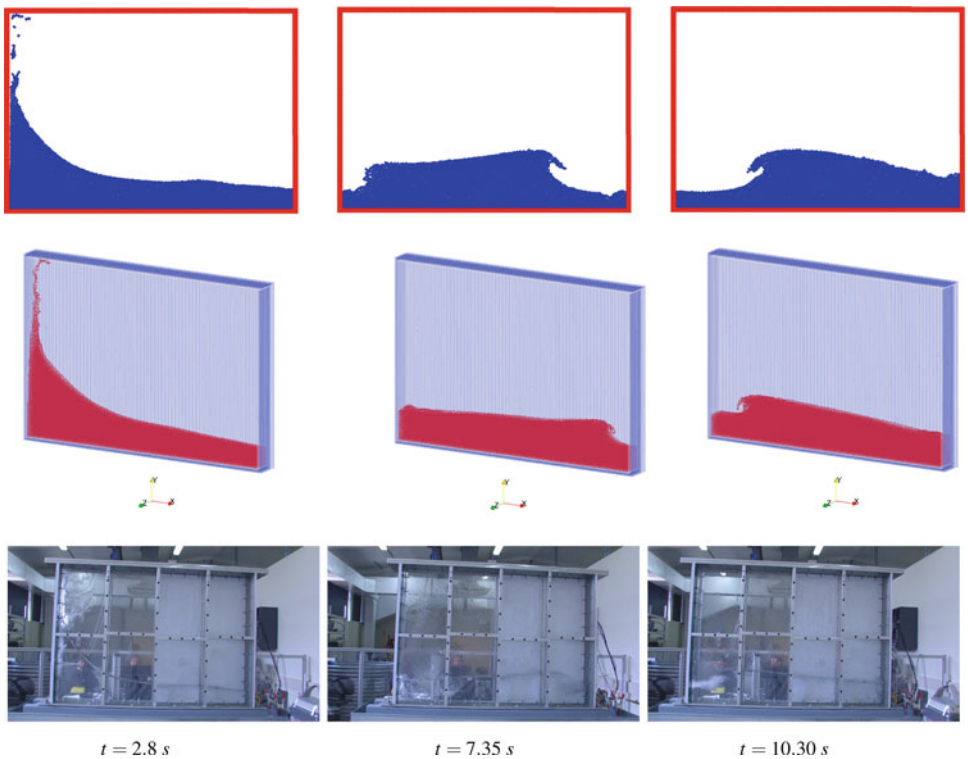

Fig. 7 The snapshots of the 2D SPH results (*first row*), 3D SPH (*second row*) and experiment (*third row*), for sloshing flow at the different times for $f = 0.496$ Hz

frequency of 60 KHz. And low pass filtered at 10 KHz through the hardware filter of the acquisition cards. Every run has the duration of 5 min.

A total number of 10 pressure transducers were used in these runs. Their positions on the side wall of the tank are shown in Fig. 4 and expressed in tank coordinates in Table 1. One of the transducers was installed in the bottom most location (number 1 in the figure and table) so to have a reference head pressure. Five transducers (numbers 6–10) have been installed around the undisturbed water level (UWL) in a cross shape arrangement in order to survey the pressure variations in the vertical direction, and in the horizontal one, so to investigate the occurrence of three dimensional effects. The remaining four transducers (numbers 2–5) have been

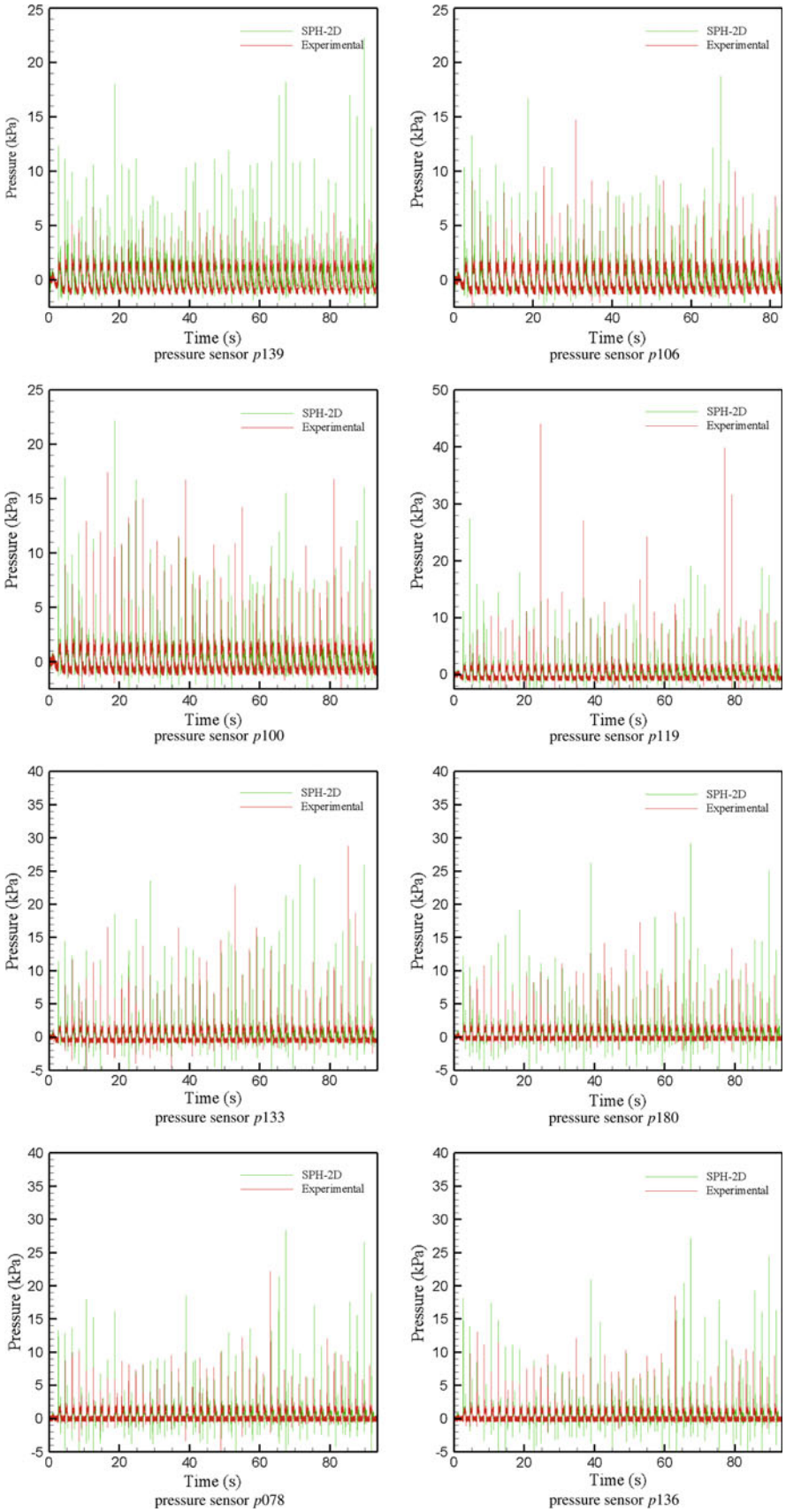

Fig. 8 Time history of pressure impact for $f = 0.496$ Hz

Table 2 Comparison of maximum of impact pressure for all sensors

	$p139$	$p106$	$p100$	$p119$	$p133$	$p180$	$p078$	$p136$
Experimental pressure (kPa)	7.24	14.738	24.258	44.094	28.827	18.799	22.177	18.507
SPH pressure (kPa)	16.994	18.795	22.2097	27.363	26.032	26.2435	25.2014	24.486

mounted to cover an intermediate position between the bottom and the UWL, where the numerical simulations expected the maximum pressure to happen for a frequency of around 0.50 Hz, so close to the resonance frequency that it has been considered important.

At the resonance frequency the breaking wave impacts on the the wall. The low frequency run generates a standing wave with no breaking, so only the hydrostatic pressure is expected with no impact. Figure 5 shows different snap shots of impact for the two cases at different random times during impact.

The size and the motion of the tank was chosen to have a two dimensional sloshing flow, although three dimensional effects of a real flow cannot be excluded. In order to ensure that this condition is preserved up to an acceptable level, three transducers have been positioned at the same horizontal line, namely at the UWL, see Fig. 4. It is observed that however the three dimensionality effects in the sloshing flow cannot truly be excluded and it is particulary significant after the first wave breaking occurs.

6 Comparison between numerical and experimental results

SPH simulations were run in 2D and 3D to compare both global and local features of the sloshing phenomenon with experimental data. For 2D SPH calculations, the particles were placed on a grid of square with initial spacing of $l_0 = 5 \times 10^{-3}$m. Whereas for 3D simulation the particles were placed on a cubic grid with initial spacing of $l_0 = 6 \times 10^{-3}$m. The smoothing length was set to $h = 1.5 l_0$ for both 2D and 3D simulations. The maximum speed inside the flow is considered to be the maximum of following two velocities

$$\begin{cases} V_1 = \sqrt{gH} \\ V_2 = \sqrt{\frac{gL}{2\pi} \tanh \frac{2\pi H}{L}} \end{cases} \tag{16}$$

where V_1 is the dispersion velocity in shallow water and V_2 is phase speed of the surface wave also called celerity. H is the depth of water in the tank and the gravitational acceleration is $\mathbf{g} = 9.81$. For numerical stability, the simulations were run at the Reynolds number of $Re = 1000$, where $Re = (2g)^{1/2} H^{3/2}/\nu$.

As expected and mentioned in previous works [40,49], the free-surface motion representative of the global behavior of the flow, is well reproduced by SPH method. Figures 6, 7 show the free-surface profile for the different frequencies. The agreement is good even for highly non-linear phenomenon such as impact on the wall.

In order to check the accuracy of the proposed technique in evaluating the local phenomenon, the impact pressure at the position of pressure sensors in the experiment were measured and compared against experimental data for the resonant condition, Frequency of $f = 0.496$ Hz. Figure 8 shows the time history of the impact pressure. It can be seen that the maximum pressure obtained by SPH method is larger than experimental data. This maybe due to the fact that the simulations are mono-phase while in the experiments, the presence of the gas (air) phase smoothes the impact pressures. Another reason to this discrepancies can be associated to the three-dimensionality nature of the sloshing flow, while the simulations were run in two-dimensions. It can be seen from the results that the secondary impact at each cycle is very well reproduced by SPH method. This can be improved by adding the second phase in SPH simulations. However, the global shape of the pressure history is very well reproduced by the proposed SPH method and is in a very good agreement with the experimental data. However, it should be noted that the impact pressure in the sloshing flow is stochastic and varies from cycle to cycle and therefore a very close agreement between numerical and experimental results is not possible. In order to have a better comparison between 2D SPH simulations and experimental data of time variation of impact pressure, the maximum of impact pressure for all sensors during 100 s of tank motion are compared in Table 2.

To further investigate the 3D effects in the numerical simulation of sloshing, the time history of the impact pressure is also plotted for the 3D simulations. Figure 9 shows the comparison of the variation of impact pressure between experimental data, 2D and 3D SPH simulations. It is observed that the impact pressure is over estimated in 2D simulation and the 3D results are in better agreement with experiment.

In the sloshing context, the variation of kinetic energy is of significant interest in tuned liquid dampers. However in this work the time history of the kinetic energy is also studied to understand how the kinetic energy transfers from liquid to the tank frame. Since the energy is given into the fluid from the motion plat form continuously, a very precise conclusion on the variation of kinetic energy is not possible. However a slight decay in the amplitude of the kinetic energy can be observed in the Figs. 10 and 11. This is associated with the

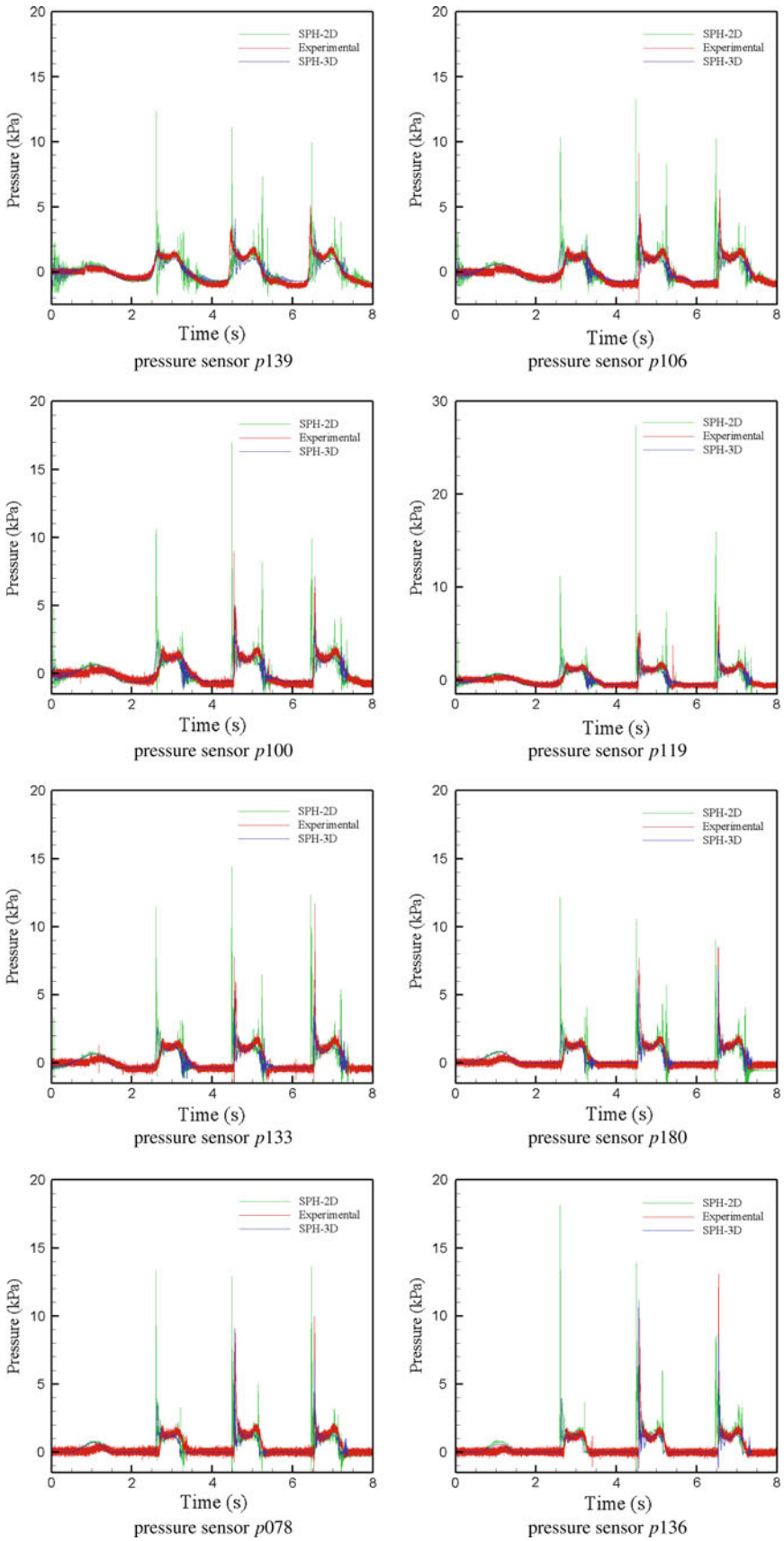

Fig. 9 Comparison of variation of impact pressure between experimental, 2D and 3D simulations for $f = 0.496$ Hz

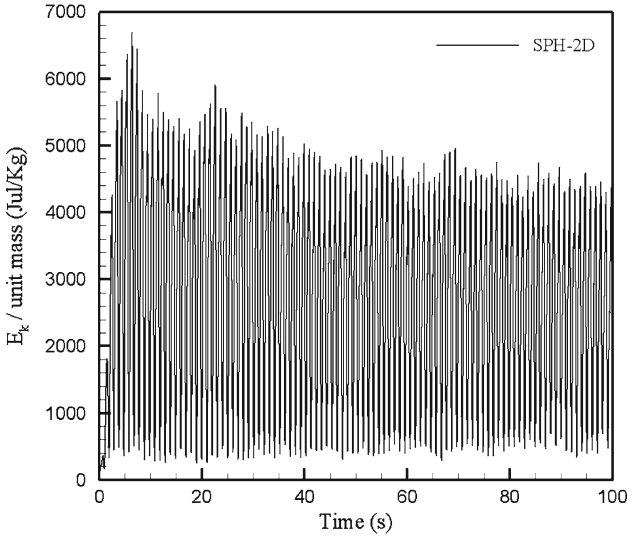

Fig. 10 Variation of kinetic energy in 2D simulation for $f = 0.496$ Hz

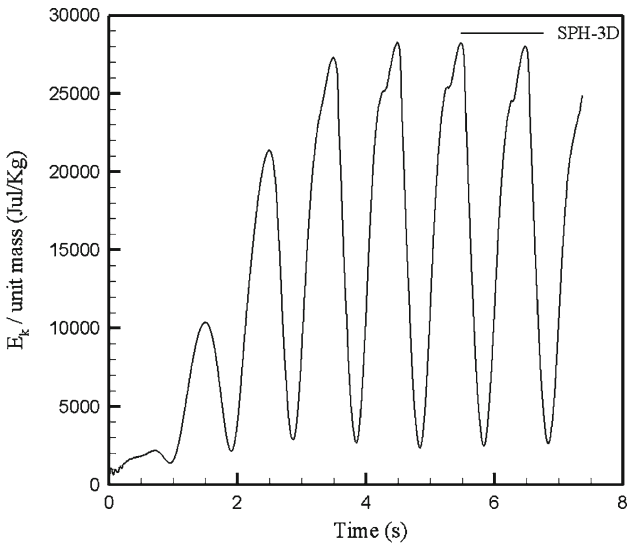

Fig. 11 Variation of kinetic energy in 3D simulation for $f = 0.496$ Hz

energy dissipation due to shearing of the fluid and hence the velocity gradient in the flow [50]. The primary reason that produces velocity gradient for the $f = 0.496$ Hz is the so-called wave-wave interaction. Therefore small percentage of energy is dissipated due to wave–wave interaction and hence causes the amplitude of kinetic energy to be reduced through the simulation time.

7 Conclusion and future works

In this paper, a set of experiments along with numerical simulations were carried out for studying the sloshing phenomenon in a rectangular tank. It was observed that the SPH technique along with the proposed approach of impact pressure evaluation can very well reproduce the global and local features of the flow. It is notable that the present results of impact pressure time history show significantly less spikes compared to the other available SPH results in the literature. The simulations were carried out for both 2D and 3D and the results compared with experimental data. It is observed that the 2D simulation tends to over estimate the impact pressure and 3D simulations predict more accurate results. The results are generally in a very good agreement with experiments, however small discrepancies in the results are caused by neglecting the air phase in the numerical simulations. The accuracy of the numerical simulation can be increased by performing two-phase simulations. Therefore, a further study need to be carried out for investigation of two-phase simulations on the global and local dynamics of the sloshing flow.

Acknowledgments The theoretical and numerical part of the study was supported by an Australian Research Council Discovery Research Grant (DP0881447). The authors acknowledge the generosity of the CHEVRON company for funding the experimental part of the work. Finally, the authors would like to thank Professor J. J. Monaghan for his fruitful and constructive comments and suggestions.

References

1. Akyildiz H, Unal E (2005) Experimental investigation of pressure distribution on a rectangular tank due to the liquid sloshing. Ocean Eng 32:1503–1516
2. Kim Y, Shin Y, Lee KH (2005) Numerical study on sloshing-induced impact pressures on three-dimensional prismatic tanks. Appl Ocean Res 26:213–226
3. Kim Y (2001) Numerical simulation of sloshing flows with impact load. Appl Ocean Res 23:53–56
4. Lee T, Zhou Z, Cao Y (2002) Numerical simulations of hydraulic jumps in water sloshing and water impacting. ASME J Fluids Eng 124:215–226
5. Mikelis NE, Miller JK, Taylor KV (1984) Sloshing in partially filled liquid tanks and its effect on ship motions: numerical simulation and experimental verification. Trans R Inst Naval Architects 126:267–277
6. Graham EW, Rodriguez AM (1952) The characteristics of fuel motion which affects airplane dynamics. J Appl Mech 19:381–388
7. Lewison GRG (1976) Optimum design of passive roll stabiliser tanks. RINA Trans Annu Rep 19:31–45
8. Aliabadi S, Johnson A, Abedi J (2003) Comparison of finite element and pendulum models for simulation of sloshing. Computat Fluids 32:535–545
9. Faltinsen OM, Rognebakke OF, Timokha AN (2005) Resonant three-dimensional nonlinear sloshing in a square-base basin. part 2: effect of higher modes. J Fluid Mech 523:199–218
10. Stoker JJ (1957) vol 4, Wiley, New York
11. Verhagen JHG, Wijngaarden L (1965) Non-linear oscillations of fluid in a container. J Fluid Mech 22:737–751
12. Abramson HN (1966) The dynamic behavior of liquids in moving containers, with applications to space vehicle technology, Technical Report SP-106, National Aeronautics and Space Administration

13. Bass RL, Bowles EB, Trundell RW, Navickas J, Peck JC, Yoshimura N, Endo S, Pots BFM (1985) Modeling criteria for scaled lng sloshing experiments. Trans Am Soc Mech Eng 107:272–280
14. Frandsen JB (2004) Sloshing motions in excited tanks. J Comput Phys 196:53–87
15. Celebi MS, Akyildiz H (2002) Nonlinear modelling of liquid sloshing in a moving rectangular tanks. Ocean Eng 29:1527–1553
16. Sames PC, Marcouly D, Schellin TE (2002) Sloshing in rectangular and cylindrical tanks. J Ship Res 46:186–200
17. Lucy LB (1977) A numerical approach to the testing of the fission hypothesis. Astron J 82:1013–1020
18. Gingold RA, Monaghan JJ (1977) Smoothed particle hydrodnamics: theory and application to nonspherical stars. Mon Not R Astr Soc 181:375–389
19. Monaghan JJ, Gingold RA (1983) Shock simulation by the particle method SPH. J Comput Phys 52:374–389
20. Benz W (1988) Applications of smoothed particle hydrodynamics (SPH) to astrophysical problems. Comput Phys Commun 48: 130–139
21. Durisen RH, Gingold RA, Boss AP (1986) Dynamic fission instabilities in rapidly rotating $n = 3/2$ polytropes: A comparison of results from finite–difference and smoothed particle hydrodynamics codes. Astron J 305:281–308
22. Monaghan JJ (1990) Modeling the universe. In: Proceedings of the Astronomical Society of Australia, vol 18, pp 233–237
23. Monaghan JJ, Lattanzio JC (1991) A simulation of the collapse and fragmentation of cooling molecular clouds. Astrophys J 375: 177–189
24. Herant M, Benz W (1991) Hydrodynamical instabilities and mixing in sn 1987a—two-dimensional simulations of the first 3 months. Astrophys J 370:81–84
25. Monaghan JJ (1992) Smoothed particle hydrodynamics. Annu Rev Astron Astrophys 30:543–574
26. Faber J, Rasio FA (2000) Post newtonian SPH calculations of binary neutron stars coalescence. Method and first results. Phys Rev D 62:1–23
27. Faber J, Manor JB (2001) Post newtonian SPH calculations of binary neutron star coalescence. ii. mass-ratio. Phys Rev D 63:1–16
28. Monaghan JJ (1994) Simulating free surface flows with SPH. J Comput Phys 110:399–406
29. Monaghan JJ (1996) Gravity currents and solitary waves. Phys D 98:523–533
30. Monaghan JJ, Cas RF, Kos A, Hallworth M (1999) Gravity currents descending a ramp in a stratified tank. J Fluid Mech 379: 39–70
31. Swegle JW, Hicks SW, Attaway S (1995) moothed particle hydrodynamics stability analysis. J Comp Phys 116:123–134
32. Libersky LD, Petscheck AG (1993) High strain lagrangian hydrodynamics- a three–dimensional SPH code for dynamic material response. J Comput Phys 109:67–75
33. Benz W, Asphaug E (1993) Explicit 3D continuum fracture modeling with smoothed particle hydrodynamics. In: Proceedings of twenty- fourth lunar and planetary science conference, pp 99–100
34. Benz W, Asphaug E (1994) Impact simulations with fracture. I. Methods and tests. ICARUS 107:98–116
35. Benz W, Asphaug E (1995) Simulations of brittle solids using smoothed particle hydrodynamics. Comput Phys Commun 87:253–265
36. Bonet J, Kulasegaram S (2000) Corrections and stabilization of smooth particle hydrodynamics methods with applications in metal forming simulations. Int J Numer Methods Eng 47:1189–1214
37. Rabczuk T, Garcie R, Song JH, Belytschko T (2009) Immersed particle method for fluid. Structure interaction. Int J Numer Methods Eng 81:48–71
38. Maurel B, Potapov S, Fabis J (2009) A Combescure, full SPH fluid–shell interaction for leakage simulation. Int J Numer Methods Eng 80:210–234
39. Rafiee A, Thiagarajan KP (2009) An SPH projection method for simulating fluid–hypoelastic structure interaction. Comput Methods Appl Mech Eng 198:2785–2795
40. Delorme L, Colagrossi A, Souto-Iglesias A, Zamora-Rodriguez R, Botia-Verra E (2008) A set of canonical problems in sloshing part I: pressure field in forced roll comparison between experimental results and SPH. Ocean Eng 36:168–178
41. Colagrossi A (2005) A meshless lagrangian method for freesurface and interface flows with fragmentation, Ph.D. thesis, Department of Mechanical Engineering, University of Rome
42. Souto-Iglesias A, Perez-Rojas L, Zamora-Rodriguez R (2004) Simulation of anti-roll tanks and sloshing type problems with smoothed particle hydrodynamics. Ocean Eng 31:1169–1192
43. Monaghan JJ (2005) Smoothed particle hydrodynamics. Rep Progr Phys 68:1703–1759
44. Batchelor GK (1974) Cambridge University Press, Cambridge
45. Morris JP, Fox PJ, Zhu Y (1997) Modeling low reynolds number incompressible flows using SPH. J Comput Phys 136:214–226
46. Souto-Iglesias A, Delorme L, Perez-Rojas L, Abril-Perez S (2006) Liquid moment amplitude assessment in sloshing type problems with SPH. Ocean Eng 33:1462–1484
47. Oger G (2006) Aspects thoriques de la mthode SPH et application lhydrodynamique surface libre, Ph.D. thesis, Ecole Centrale de Nantes, France
48. Molteni D, Colagrossi A (2009) A simple procedure to improve the pressure evaluation in hydrodynamic context using the SPH. Comput Phys Commun 180:861–872
49. Rafiee A, Thiagarajan KP, Monaghan JJ SPH simulation of 2D sloshing flow in a rectangular tank. The 19th international offshore and polar engineering conference (ISOPE)
50. Marsh A, Prakash M, Semercigil E, Turan OF (2010) A numerical investigation of energy dissipation with a shallow depth sloshing absorber. Appl Math Model 34:2941–2957